J. Phys. Chem. Solids Vol. 52, No. 1, pp. 211–225, 1991
Printed in Great Britain.

0022-3697/91 $3.00 + 0.00
Pergamon Press plc

SPECTROSCOPIC PROPERTIES OF DEFECTS IN ALKALINE-EARTH SULFIDES

RAVINDRA PANDEY† and S. SIVARAMAN‡
†Department of Physics, Michigan Technological University, Houghton, MI 49931, U.S.A.
‡Department of Physics, University of Saugar, Sagar, M.P., India 470003

Abstract—Spectroscopic properties of pure and impurity-activated alkaline-earth sulfides as studied by optical and magnetic resonance techniques are reviewed.

Keywords: Alkaline-earth sulfides, defects.

1. INTRODUCTION

Alkaline-earth sulfides have recently been the subject of renewed interest both theoretically [1] and experimentally [2], because of their potential as host materials for device applications such as multi-color thin film electroluminescent [3] and magneto-optical devices [4].

Although sulfides are one of the oldest luminescent materials, studied first by Lenard *et al.* in 1928 primarily for infra-red applications [5], there is a comparative dearth of information about defect properties in these materials. The primary reason for this under-representation in the literature is the relatively high melting temperatures ($\sim$2300 K) of these materials presenting severe difficulty in growing them as single crystals. Thus polycrystalline forms of sulfides have generally been used to study defect properties leading to sometimes contradictory and inconclusive results.

In 1972, Lehmann and Lehmann and Ryan [6, 7] reported the results of a detailed and systematic investigation in CaS concluding that it is an excellent host material for efficient cathode-ray tube phosphors when activated with rare earths. Since then a number of reports have appeared describing spectroscopic properties of pure and activated sulfides and revealing applications of BaS, SrS and MgS in alloy semiconductors [8], radiation dosimetry [9] and fast high-resolution optically-stimulated luminescence imaging [10]. However, no attempt has so far been made to summarize the results of spectroscopic studies on sulfides scattered around in the literature. In this article we propose to fill this gap by reviewing the results that have been obtained since 1972. In doing so, we shall try to describe the way in which the spectroscopic properties of impurities alter as one proceeds from BaS to MgS. We shall also try to understand the role of intrinsic defects governing the physical properties which make them useful for device applications. We note here that the preparation techniques and thermoluminescent behavior of sulfides have recently been reviewed by RaO [11].

2. PURE (UNACTIVATED) SULFIDES

Sulfides have the face-centered cubic NaCl structure and are characterized by a high degree of ionicity. The ionic character may be measured empirically from the (fractional) ionicity [12] or Szigetti's effective charge (Z_s^*) derived from the experimental values of the dielectric constants and the phonon frequency, ω_{TO} [13]. The ionicity is fairly large (0.8–0.9) and the effective charge Z_s^* is around 1.0 indicating that sulfides are predominantly ionic in character. Furthermore, Pandey *et al.* [1, 14] have successfully used the ionic description to provide a framework for defect simulation in sulfides.

Experimental band-gap energies of sulfides determined from the optical reflection spectra by various workers [6, 15, 16] are listed in Table 1. *Ab-initio* band structure calculations [80] predict that sulfides (except MgS) are direct gap materials, contrary to what has been suggested by Kaneko and Koda [2].

The optical reflection spectra of sulfides are dominated by peaks assigned to excitonic-type transitions (Fig. 1). Table 2 lists the observed excitonic energies indicating a satisfactory agreement between the values obtained from thin film and single crystals of sulfides. The excitonic transition may be described in terms of transitions from the ground state configuration $3p^6$ of S^{2-} ions to the $3p^5 4s$ state. The splittings between the first two strong peaks may then be attributed to the spin–orbit splitting associated with the hole on the S^{2-} ion. The observed splitting is of the order of 0.06, 0.09 and 0.14 eV in CaS, SrS and BaS, respectively, in comparison with the estimated splitting of about 0.11 eV [18]. Higher energy peaks may be associated with transitions to higher excited states in sulfides.

Table 1. Experimental band-gap energies of sulfides

	MgS	CaS	SrS	BaS
Band-gap (eV)				
Polycrystalline, 300 K†	5.4	4.8	4.4	3.8
Single crystal, 77 K‡	—	5.3	—	—
Single crystal, 2 K§	—	5.343	4.831	3.941
Lattice constant (a)	5.204¶	5.6975‖	6.0190‖	6.3842‖

† Lehmann and Ryan [7].
‡ Realo and Jaek [16].
§ Kaneko and Koda [15].
¶ Quoted by Thakur and Pandey [17].
‖ Kaneko *et al.* [13].

The infra-red spectra of sulfides measured from 50 to 400 cm^{-1} are composed of a main reststrahlen band and a subsidiary band on the higher energy side of the former (Fig. 2). The subsidiary bands at about 395 and 250 cm^{-1} in SrS and BaS, respectively, are attributed to the third-order anharmonicity in the lattice potential. Dispersion analysis of the reststrahlen band based on a classical oscillator model yields the phonon frequency ω_{TO} of about 229, 185, and 150 cm^{-1} for CaS, SrS and BaS, respectively, suggesting that the optical phonons in sulfides can be treated in the central-force model. The phonon frequency ω_{LO} derived from a Lyddane–Sachs–Teller relation, $\omega_{LO}/\omega_{TO} = \sqrt{\epsilon_0/\epsilon_\infty}$, is 342, 282, and 246 cm^{-1} for CaS, SrS and BaS, respectively [13].

3. INTRINSIC POINT-DEFECTS

Evidence of intrinsic point-defects in sulfides was first obtained by Auzins *et al.* using the electron paramagnetic resonance (EPR) technique [19]. In CaS, Ghosh and his coworkers reported two kinds of photosensitive EPR signals at $g = 1.9998$ and 2.00018 arising from sulfur vacancies (Fig. 3). The sulfur vacancy (which is doubly positively charged in the lattice) traps an electron released from the lattice by photoexcitation, thereby becoming a paramagnetic center. The observed difference in the g-values may be due to the different surrounding around the EPR center in the lattice. For example, a calcium vacancy near to the EPR center may be present in the lattice [20, 21]. Ghosh and Pandey [22] have identified calcium vacancies in the lattice by analyzing thermoluminescence glow-curves but no direct evidence has so far been obtained.

3.1. F^+/F *center*

In X-ray-irradiated CaS at room temperature, the EPR spectrum consists of an intense signal at $g = 2.0032$ attributed to the F^+ center [20]. Single crystals of BaS irradiated with neutrons (>1 MeV) have also produced the F^+ center signal at $g = 1.9637$ [23]. The isotropic part of the hyperfine interaction A was found to be 41.0 and 36.4 G for the nearest-neighbor ^{137}Ba and ^{135}Ba nuclei, respectively. It is interesting to note here that the corresponding g-values of the F^+ center in oxides, CaO and BaO, are 2.0001 and 1.9355, respectively. Also, Ekbote and Ranade have observed EPR signals at $g = 1.997$ and 2.05 in CaS with $CaCl_2$ flux [24]. They attributed these signals to sulfur-vacancy aggregate centers since sulfurization of the samples reduced the intensities of the EPR signals.

Thus several EPR centers due to sulfur vacancies have been observed, but no correlation has been established between the EPR and the optical properties in contrast to the situation in alkaline-earth oxides. This is due to the fact that the reported work on the optical properties is rather scarce and limited to the optical stimulation (excited absorption) spectrum of emission bands in pure sulfides [25].

3.1.1. *ICECAP calculation.* Since the F^+ center consists of a single trapped electron in the sulfur vacancy, we may label its electronic states as $1s, 2s, 2p, \ldots$ etc. which are analogous to those of a one-electron atom, in this case He^+. The first allowed optical transition is therefore between the $1s$ and $2p$ states. Since such a transition takes place on a time-scale short compared with lattice vibrations, it will occur while the lattice atoms remain essentially at some fixed configuration (~Franck–Condon principle). The $1s$ and $2p$ states are then referred to as the

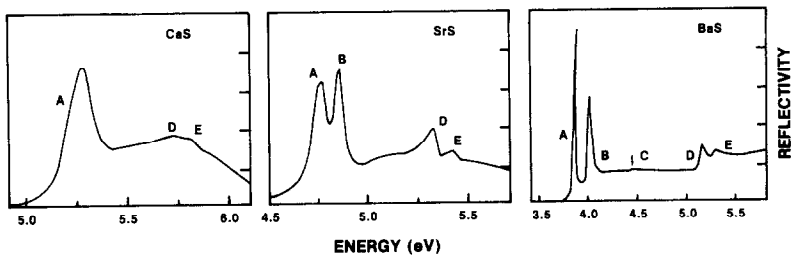

Fig. 1. Optical reflectivity spectra at 2 K. The features denoted A, B, and C are assigned to X-point excitons and those denoted D and E to Γ-point excitons (Kaneko and Koda [15]).

Table 2. Excitonic energies in sulfides

	Excitation spectrum (eV)				
CaS,					
single crystal, 2 K†	5.273	5.337	5.54	5.74	5.82
SrS,					
single crystal, 2 K†	4.761	4.855	5.49	5.321	5.425
thin film, 113 K‡	4.76	4.91	5.44		
BaS,					
single crystal, 2 K†	3.868	4.01	4.46	5.116	5.30
thin film, 113 K‡	3.88	4.03	4.48	5.10	5.25

† Kaneko and Koda [15].
‡ Zollweg [18].

ground and unrelaxed excited states for the optical absorption process of the F^+ center.

Pandey *et al.* [1] used the program package ICECAP to simulate the F^+ center in sulfides as a one-electron cluster embedded in the shell model lattice. The details of the ICECAP methodology are given by Vail in Part I of this issue. The *s*- and *p*-type basis functions are chosen to describe the ground and unrelaxed excited states, respectively. These functions are Gaussian localized $\sim\exp(-\alpha r^2)$, where α is referred to as an exponent. In the ground state, ICECAP minimizes the total energy of the trapped electron and its embedding lattice, with respect to the shell model lattice positions. In the unrelaxed excited state, it evaluates the total energy with the lattice positions frozen in the ground state configuration. Furthermore, ICECAP includes the consistent treatment of the static distortion and polarization in the surrounding lattice for these calculations. We note that the F^+ center is a charged defect in sulfides producing significant distortion and polarization in the lattice. In the present case, the nearest-neighbor cations of the F^+ center relax outward to the vacancy by 5, 3, and 2% in CaS, SrS, and BaS, respectively. The optimized range of *s*- and *p*-type Gaussians chosen to represent the ground and unrelaxed excited states of the F^+ center comes out to be $0.50a$ in all cases, where a is the nearest-neighbor spacing in the lattice.

One-electron calculations have been successful in predicting the optical absorption energy (i.e. difference between the ground state and unrelaxed excited state energies) of the F^+ center in alkaline-earth oxides [26]. Similar success may therefore be expected in alkaline-earth sulfides.

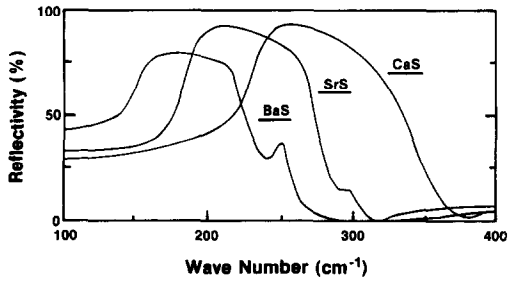

Fig. 2. Infra-red reflection spectra at room temperature (Kaneko *et al.* [13]).

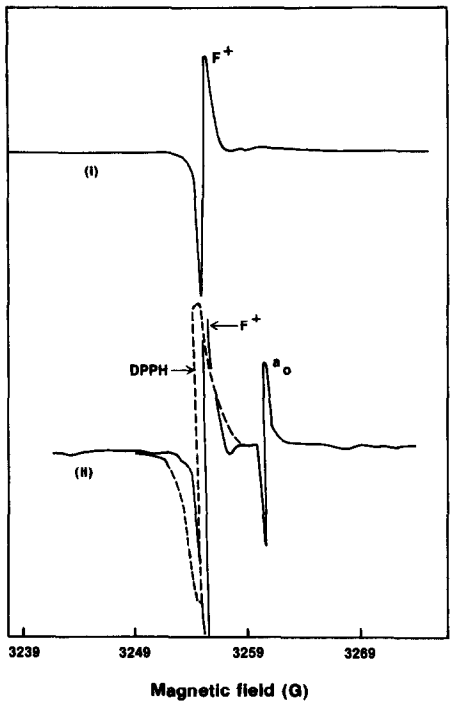

Fig. 3. EPR spectra of CaS (Shanker *et al.* [21]). (i) F^+ center signal at room temperature in X-ray irradiated CaS. (ii) Photosensitive EPR signal at 93 K in CaS.

The calculated results are given in Table 3. Referring to this table, it appears that these calculations do reproduce the optical absorption energy in calcium and strontium sulfides reasonably well. For barium sulfide, the calculation predicts absorption at 2.34 eV as compared with the somewhat doubtful experimental value of 1.94 eV, which was obtained in bismuth-activated BaS using an empirical formula [28]. On the other hand, Kapoor and Hensley have studied the optical absorption of additively-colored single crystals of BaS (Fig. 4) and have identified absorption bands at 1.77, 2.33 and 2.75 eV for the F center (i.e. sulfur vacancy containing two electrons) because they failed to observe the $F \rightarrow F^+$ photoconversion [29]. For the observed splitting of the F center band, it has been suggested that it is mainly a consequence of the *p*-like states being perturbed by the nearly *s*-like

Table 3. F^+ center absorption energy

	Absorption energy (eV)	
	Calculated	Observed
CaO	3.70	3.65†
CaS	2.63	2.60‡
SrS	2.54	2.30§
Bas	2.34	1.94¶

† Henderson, unactivated CaO crystal [26].
‡ Rebane *et al.*, unactivated polycrystalline CaS [25].
§ Efanova and Mikhailin, quoting EPR-optical absorption study in deformed SrS [27].
¶ Allsalu *et al.*, using empirical formulas in BaS : Bi[28].

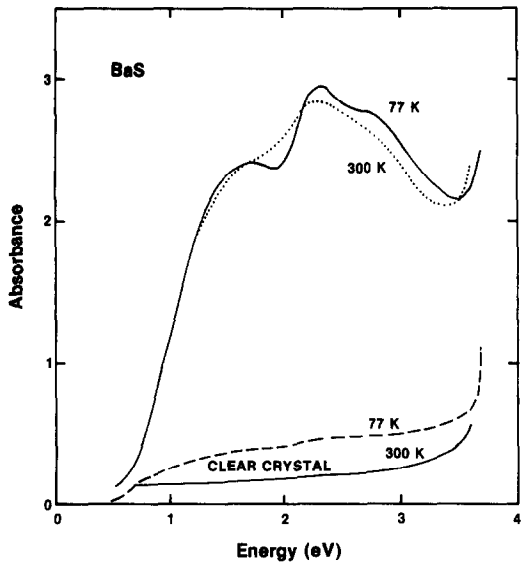

Fig. 4. Optical absorption spectra of the F center in BaS (Kapoor and Hensley [29]).

state, rather than a result of strong John–Teller interaction. Since no attempt has been made to correlate the absorption study with the EPR study, there exists the possibility of the overlap of the F and F^+ absorption bands in BaS.

3.2. *Self-activated emission*

Self-activated emission has been observed in pure sulfides (Fig. 5). Table 4 lists the peak-positions indicating that the emission spectrum depends on the preparation techniques.

Polycrystalline CaS prepared by reduction of calcium sulfate at 1273 K shows three bands at 420, 490 and 580 nm, respectively [30]. Using the same starting material but a different firing temperature (~1323 K), Ray *et al.* have observed the bands at 360, 420 and 480 nm, respectively [31]. On the other hand, CaS prepared by reducing calcium nitrate exhibits a dominant peak at 360 nm with an additional small peak at 485 nm [32]. Single crystals of CaS grown by vapor phase transport using iodine

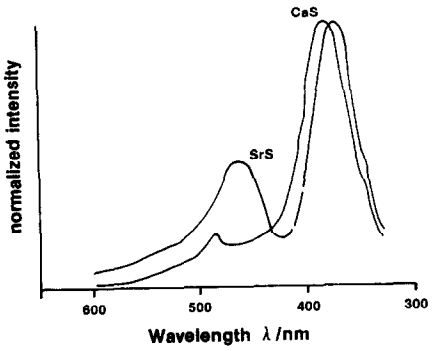

Fig. 5. Normalized emission spectra of pure sulfides at 77 K (Brightwell *et al.* [32]).

Table 4. Spectral position in the emission spectra of pure sulfides

Preparation technique	Emission spectra (nm)
CaS	
Polycrystalline,† $CaSO_4$, 300 K	420,490, 580
‡ $CaSO_4$, 300 K	360, 420, 480
§ $Ca(NO_3)_2$, 300 K	360,485
77 K	380,485
Single crystal,¶ 300 K	360, 425, 445, 485
SrS	
Polycrystalline,§ 77 K	380, 460
BaS	
Polycrystalline,‖ 80 K	450

† Ghosh and Shanker [30].
‡ Ray *et al.* [31].
§ Brightwell *et al.* [32].
¶ Brightwell *et al.* [33].
‖ Allsalu *et al.* [34].

show a principal maximum at 425 nm with shoulders at 360, 445 and 485 nm [33].

Prolonged X-ray irradiation enhanced considerably the emission peak at 580 nm in CaS. This peak has a decay time of 3 μs and it is suggested that it is associated with sulfur vacancies [30]. The peak at about 485 nm has been assigned to the presence of trace levels of oxygen in CaS. The origins of the emission bands at 360 and 420 nm are unknown but must be associated with either intrinsic defects or trace impurities present in CaS.

In SrS, the emission spectrum consists of a dominant peak at 380 nm with a broader band at 460 nm (Fig. 5). Sivaraman and Bhawalkar have also reported a band at 475 nm in SrS phosphors activated with bismuth, lead, tin, zirconium and thorium indicating that the emission is characteristic of the host lattice [35]. As Ca is introduced in the SrS lattice, the intermediate compositions show a range of emission bands from 380 to 530 nm [32]. It has been suggested that anion vacancies may be responsible for these emission bands in $Ca_xSr_{1-x}S$.

4. IMPURITIES

4.1. *Manganese*

Manganese is known to occur in pure sulfides as a natural admixture in the concentration range of about 0.35 ppm. Its valence state has been identified as +2 containing an incomplete $3d$ shell ($3d^5$), the ground state being $^6S_{5/2}$.

The characteristic sextet of Mn^{2+} corresponding to the nuclear spin of ^{55}Mn, $I = 5/2$ in sulfides has been observed having a narrow line-width (~0.25 G) and attributed to substitutional Mn^{2+} ions, with cubic symmetry in the lattice [36–40]. The spin-Hamiltonian parameters, namely the spectrosplitting factor g and isotropic hyperfine constant A for Mn^{2+} are nearly the same in Mg, Ca and Sr sulfides, indicating the same bonding character of Mn^{2+} in these sulfides (Table 5). It may be noted here that for Mn^{2+} in CaO

Table 5. Spin-Hamiltonian parameters for Mn^{2+} in sulfides

		g	$\lvert A \rvert$ ($10^{-4}\,cm^{-1}$)	λ emission
MgS:				
polycrystalline,†	300 K	2.0019	74.8	695
polycrystalline,†	77 K	2.0017	75.0	705
CaS:				
polycrystalline,‡	300 K	2.0014	84.1	—
polycrystalline,§	300 K	—	—	585.8
polycrystalline,¶	77 K	2.0014	75.3	—
single crystal,‖	300 K	—	—	575.0
single crystal,††	77 K	2.00175	77.0	—
SrS:				
polycrystalline,¶	77 K	2.0008	74.8	—

† Asano *et al.* [36].
‡ Ghosh *et al.* [37].
§ Lehmann [6].
¶ Nair *et al.* [38].
‖ Brightwell *et al.* [33].
†† Wagner *et al.* [39].

the value of A is approximately $81 \times 10^{-4}\,cm^{-1}$, compared with that of about $77 \times 10^{-4}\,cm^{-1}$ in CaS and thus suggesting the same percentage of covalent character of the bonding of Mn^{2+} in both compounds. Also the Mn^{2+}–anion bond is found to be far less covalent than in ZnS : Mn [36].

A calculation of the parameter $10Dq$ which is a measure of crystal field intensity, yields values of approx. 8170 and 6480 cm^{-1} for MgS and CaS, respectively [35]. In comparison, $10Dq$ is found to be 6800 cm^{-1} in CaO.

The emission spectra of Mn^{2+}-doped sulfides consist of single bands whose peak positions are about 580 nm in CaS and 695 nm in MgS (Fig. 6). The emission is assumed to be due to transitions from the first excited state ^4G to the ground state ^6S within the Mn^{2+} ion. The decay time associated with this yellow emission band is found to be 4 ms [37]. The excitation spectrum of the Mn^{2+} emission band consists of peaks ranging from 345 to 600 nm in MgS (Fig. 6) and 340 to 545 nm in CaS [36, 40].

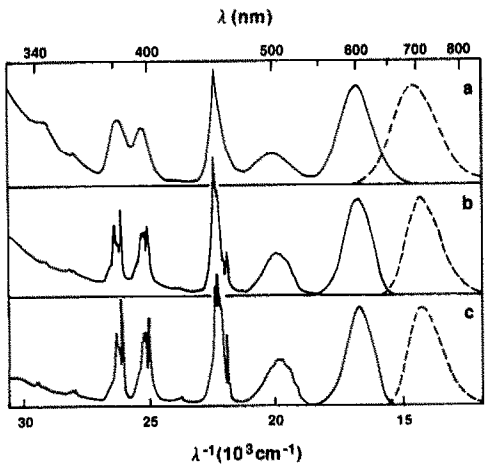

Fig. 6. Excitation and emission spectra of MgS : Mn (0.3 mol%) at (a) $T = 300$, (b) 80, and (c) 6 K (Asano *et al.* [36]).

Table 6. Spectral positions in the emission spectra of Cu-activated sulfides

		Emission spectrum (nm)
MgS:	Cu†	432
	Cu, Na	442
CaS:	Cu†	416, 491
	Cu, Li	412, 486
	Cu, Na	442, 493
	Cu, K	419, 487
	Cu, Rb	422, 482
	Cu, F	420, 477
	Cu, P	414, 482
	Cu, As	424, 491
SrS:	Cu‡	471, 517, 548
SrS:	Cu†	466, 515
	Cu, Na	536
BaS:	Cu§	568
BaS:	Cu§	589
	Cu, Na	609

† Lehmann [4].
‡ Laud and Kulkarni [42].
§ Laud and Kulkarni [43].

4.2. *Copper*

The work so far reported on Cu-activated sulfides is limited to emission studies [41–43]. The emission spectrum strongly depends on the presence of a coactivator in the lattice influencing the peak-positions of the emission bands (Table 6). However, no systematic trend in the peak-shift has been observed as either the host lattice (Fig. 7) or coactivators are varied [41].

The Cu emission also depends on the Cu concentration in the lattice and shows concentration quenching at higher Cu concentrations. In CaS the

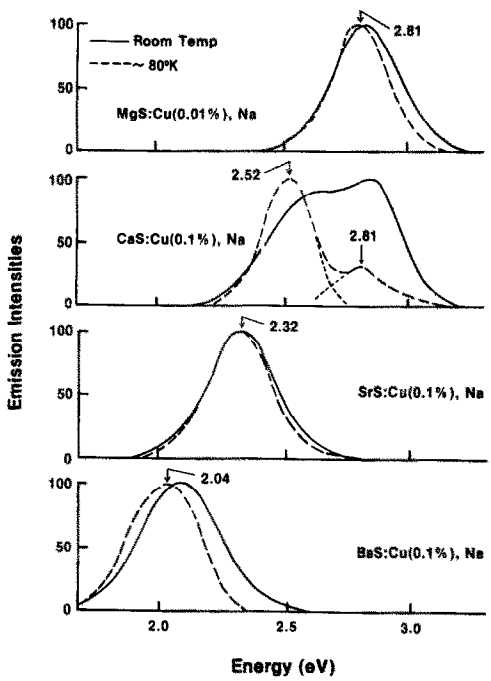

Fig. 7. Emission spectra of Cu-activated sufides (Lehmann [41]).

spectrum consists of two bands at about 442 and 493 nm disappearing at high Cu concentration (>0.5 mol%), when a broad band appears at about 530 nm [41]. In SrS the spectrum consists of three bands at about 471, 517 and 548 nm at low Cu concentration (~0.01 mol%) [41]. In BaS the main emission band at 568 nm shifts to 570.5 nm for high Cu concentration. In mixed sulfides, SrS–BaS, a gradual shift of the emission spectra to longer wavelengths with increasing BaS content was observed as expected [43].

The emission bands in Cu-activated sulfides are attributed to Cu^+ ions in the lattice. The proposed models to explain Cu emission are based on models for ZnS : Cu phosphor. For example, the blue band at 471 nm in SrS is attributed to a Cu^+ ion in an interstitial site, as has been suggested for the blue emission of Cu in ZnS [42]. The green and yellow emission bands of Cu are attributed to substitutional Cu^+ in the lattice replacing the host cation. Furthermore, the dependence of the emission spectrum on the coactivator is explained on the basis of activator–coactivator pairs, as also suggested for all the main emission bands of Cu in ZnS [41].

4.3. *Silver and gold*

There has not been any work done on Ag- and Au-activated sulfides since Lehmann's study [41].

Silver is found to be an inefficient activator in sulfides. On the other hand, Au-activated sulfides are found to be as efficient as Cu-activated sulfides with the exception of MgS. It seems that Au with an ionic radius of 1.37 Å is too big to replace the Mg^{2+} ion with an ionic radius of 0.65 Å in MgS. The peak-positions of the emission bands are listed in Table 7. The emission spectra depend on the coactivator in Cu-activated sulfides.

4.4. *Arsenic and phosphorus*

Both these activators require the addition of a halide ion as coactivator and a reducing firing atmosphere for the preparation of the phosphor. In CaS, phosphorus induces an emission band at about 583 nm whereas arsenic induces a band at about 621 nm [6]. However, Ghosh and Jain have failed to observe an emission band associated with As and have suggested that As acts as a sensitizer for the self-activated emission of CaS [44].

Table 7. Spectral positions in the emission spectrum of Ag- and Au-activated sulfides

		Emission spectrum (nm)
Ag, K†:	MgS	439
	CaS	338
	SrS	432
	BaS	466, 550
Au, K†:	MgS	Non-luminescent
	CaS	515, 578
	SrS	485, 570
	BaS	665

† Lehmann [41].

4.5. *Cadmium*

CdS can form solid solutions with CaS, replacing up to 55% of CaS while retaining the NaCl structure [6]. The optical absorption edge decreases linearly as the Cd content is increased in the mixed crystal $Ca_{1-x}Cd_xS$. For low Cd concentration, the emission spectrum consists of peaks at 290, 335, 360, 420 and 480 nm [31]. With increasing Cd concentration, the peaks show broadening and the spectrum now extends from 310 to 825 nm [6]. It has been suggested that at high Cd concentration in CaS, clustering of Cd ions may occur causing local lattice distortion which may then act as emission centers in $Ca_{1-x}Cd_xS$.

4.6. *Bismuth*

Bismuth is a well-characterized impurity center in sulfides. Its optical properties have been studied in great detail by a group led by Asano and Yamashita, who identified the excitation and emission bands as due to substitutional Bi^{3+} ions in the lattice [45–50]. The Bi^{3+} is one of the ns^2 impurities like Tl^+, Ga^+, In^+, Sn^{2+}, Pb^{2+} and Sb^{3+}. The lowest energy absorption bands can be assigned to the transition from the ns^2 ground state to the $nsnp$ excited state. In a cubic crystal field the energy levels of the $nsnp$ configuration are split into the $^3A_{1u}$, $^3T_{1u}$, $^3E_u + {}^3T_{2u}$ and $^1T_{1u}$ terms. The absorption (excitation) bands, generally known as A, B and C in order of increasing energy, correspond to the transitions from the $ns^2(^1A_{1g})$ ground state to the $^3T_{1u}$, $^3E_u + {}^3T_{2u}$ and $^1T_{1u}$ terms, respectively. Table 8 lists the peak-positions of the excitation bands observed in Bi-activated sulfides and Fig. 8 shows the excitation and emission spectra obtained at 80 K in SrS : Bi.

The emission spectra of Bi-activated sulfides consist mainly of a blue band at room temperature splitting into two bands, I and II, at low temperature. These overlapping bands can only be separated by using time-resolved spectroscopy. In SrS decay measurements have revealed that band I has a decay time constant of about 10 ns while for band II it is of the order of milliseconds [50]. Both bands are nearly equal in intensity under A-band excitation (~420 nm) but under C-band excitation (~330 nm) band II is more prominent (Fig. 9). Furthermore, the relative intensities of both bands vary with temperature such that above 150 K only band I remains. Thus the results for band II (with a long decay time and temperature dependent intensity) suggest that the transition $^3A_{1u} \rightarrow {}^1A_{1g}$, supposedly strongly forbidden, is responsible for band II [50]. (Compare the article by Jacobs in this special issue.)

In BaS, Asano *et al.* have observed only one emission band at 561 nm and have assigned it to the transition $^3A_{1u} \rightarrow {}^1A_{1g}$ (i.e. band II). According to

Table 8. Spectral positions in the excitation and emission spectra of Bi-activated sulfides

		Excitation spectrum (nm)	Emission spectrum (nm)
MgS,	300 K†	—	440
	80 K	324, 348, 417	428, 446
CaS,	300 K‡	414	448
	63 K§	307, 411	434, 452
	6 K¶	312, 347, 412	437, 450
SrS,	300 K‖	—	486
	80 K‖	330, 420	475, 488
	63 K§	431	478*
BaS,	300 K††	370, 448	561
	80 K‡‡	371, 447	552

* Overlapping bands with different decay time constant.
† Asano and Yamashita [47].
‡ Lehmann [6].
§ Ellervee [52].
¶ Yamashita and Asano [45].
‖ Yamashita *et al.* [50].
†† Asano *et al.* [48].
‡‡ Efanova [51].

them, the emission band I (which is associated with the transition $^3T_{1u} \rightarrow {}^1A_{1g}$) cannot be observed due to the fact that the tunneling probability from the $^3T_{1u}$ to the $^3A_{1u}$ state is larger than that of the radiative transition to the $^1A_{1g}$ state [48]. Referring to Table 8, we note that the Stokes shift corresponding to the transition $^1A_{1g} \leftrightarrow {}^3T_{1u}$ depends on the host lattice being 11 nm in MgS, 25 nm in CaS, and 55 nm in SrS.

Both the excitation and emission spectra of Bi-activated sulfides are found to exhibit phonon structure at 6 K [46–48, 50]. A zero-phonon line common to both the excitation A band and the emission I band is observed. It is referred to as the zero-phonon line, T_0^1 of the $^1A_{1g} \leftrightarrow {}^3T_{1u}$ transition. The weak zero-phonon line A_0 and the intense one-phonon line A_0^1 of emission band II (due to the transitions from the zero-phonon level of the $^3A_{1u}$ state to the zero- and one-phonon levels of the $^1A_{1g}$ state, respectively) have also been reported.

In the absence of an external magnetic field, the weak A_0 line may arise either from the hyperfine interaction between the nuclear spin and electrons in the activator Bi^{3+} ion [49] or from the static perturbation resulting from the distorted crystal field caused by introducing the activator Bi^{3+} ion into the lattice [52]. In a more detailed study, Yamashita and Asano have shown that the appearance of the A_0 line is exclusively due to the hyperfine interaction [53]. In a magnetic field, the intensity of the A_0 line is found to increase in proportion to the square of the magnetic field [49].

It has been suggested that the strongly forbidden transition $^3A_{1u} \rightarrow {}^1A_{1g}$ may be allowed due to the mixing of the $^3T_{1u}$ state with the $^3A_{1u}$ state through the magnetic electron–phonon interaction induced by the T_{1g} vibrational mode. Asano has shown that ordinary electric electron–phonon interaction has no affect on the admixture of these states [47b]. The distance between the A_0 and A_0' lines can then be attributed to the phonon energy $\hbar\omega_g$ with the T_{1g} mode in Bi-activated sulfides.

In Table 9 the positions of the phonon lines and the phonon energy $\hbar\omega_g$ are given for Bi-activated sulfides.

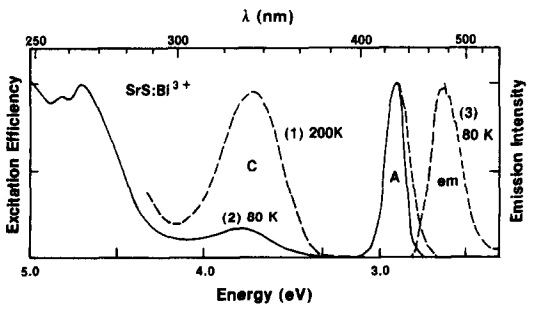

Fig. 8. (1), (2)—Excitation spectra observed at 488 nm, the emission band II. (3)—Emission spectra under steady excitation at 420 nm, A band (Yamashita *et al.* [50]).

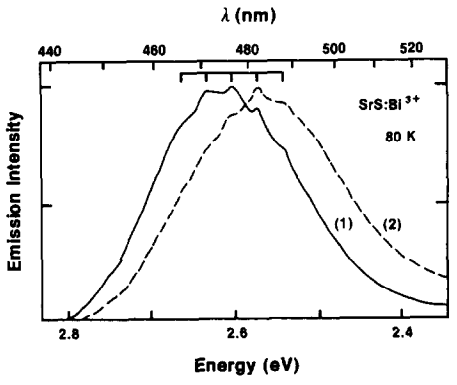

Fig. 9. Emission spectra of SrS : Bi (0.05 mol%) at 80 K under steady excitation (1) at 420 nm, A band (2) at 330 nm, C band (Yamashita *et al.* [50]).

Table 9. Spectral positions of the zero-phonon lines and the phonon energy $\hbar\omega_g$ for the Bi^{3+} and Pb^{2+} centers in sulfides

		T_0 (nm)	A_0 (nm)	$\hbar\omega_g$ (cm^{-1})
Bi^{3+}:	MgS†	420.4	437.1	177
	CaS	422.1	437.1	207
	SrS	445.3	460.7	200
	BaS	479.6	491.2	184
Pb^{2+}:	MgS‡	357.1	368.7	178
	CaS	347.2	357.9	225
	SrS	355.2	365.3	201

† Asano *et al.* [48].
‡ Yamashita *et al.* [55].

We note here that the TO and LO phonons in sulfides are reported to be 185 and 282 cm^{-1}, respectively [13]. It is therefore reasonable to assume that vibrational modes coupled to the electronic transition in the Bi^{3+} ion are localized modes. Table 9 also includes the results of Pb^{2+}-activated sulfides indicating that the phonon energy $\hbar\omega_g$ is independent of the activator ion in the sulfides. A rigid rotation model can then be applied to calculate the T_{1g} mode corresponding to the rotational vibration of the octahedral complex. The octahedral complex consists of the activator ion and its six nearest-neighbors behaving as if it were a rigid rotator bound to the host lattice with a restoring force obeying Hooke's law. Calculated values of the frequency of the T_{1g} mode agree satisfactorily with experiment for Pb^{2+}-activated sulfides [55].

The activation of Bi^{3+} in sulfides may require coactivation by monovalent alkali ions indicating substitution of two host cations by pairs of Bi^{3+} and the alkali ion. It has been shown that the peak positions of the emission bands are not changed by the presence of the coactivator. However, the presence of coactivator does affect the intensities of the emission bands [52]. Furthermore, Asano and Yamashita have reported additional excitation and emission bands originating from the associated centers Bi^{3+}–Li^+ in addition to those of a single Bi^{3+} center in CaS [45].

4.7. *Lead*

Both the excitation and emission spectra of Pb-activated sulfides show a strong similarity with those of Bi-activated sulfides. The excitation spectrum consists of the *A*, *B* and *C* bands corresponding to the transitions from the $5s^2$ ground state to the energy levels of the $5s5p$ excited state of the Pb^{2+} ion whereas the emission bands are identified with $^3T_{1u} \rightarrow {}^1A_{1g}$ and $^3A_{1u} \rightarrow {}^1A_{1g}$ transitions, respectively [51, 53–55]. However, the Stokes shift associated with the $^3T_{1u} \leftrightarrow {}^1A_{1g}$ transition shows very little variation in sulfides in contrast to what has been observed in Bi-activated sulfides (Table 10).

Pb^{2+} ion can be incorporated easily into sulfides, specifically into CaS due to the isomorphism of the crystal structures of CaS and PbS. Dimer and higher aggregate centers tend to form abundantly in the lattice with increasing concentration of Pb^{2+} ions. No concentration quenching of the emission intensity has been observed and even CaS activated with 20 mol% of PbS is found to be luminescent [56]. With increasing Pb^{2+} concentration, additional bands in both excitation and emission are observed and these are attributed to electronic transitions in the [110] dimer of the Pb^{2+} ion. Furthermore, it has been observed that the excitation energy absorbed by the host sulfide is transferred to the dimer centers more efficiently than to single Pb^{2+} centers in the lattice [56].

A rich vibrational structure appears in the spectra of Pb-activated sulfides at low temperatures showing a similarity with that observed in Bi-activated sulfides. Table 9 lists the positions of the zero-phonon lines and the phonon energy associated with the T_{1g} mode. We note here that the zero-phonon lines are almost independent of the host sulfides. This is in contrast to the situation for Bi-activated sulfides for which the positions of the zero-phonon lines show a relatively larger separation.

4.8. *Tin*

Jaek *et al.* have carried out a detailed study measuring Mössbauer, EPR and optical spectra of Sn centers in CaS [58]. The relative intensities of the Sn-induced emission bands at 388 and 539 nm in CaS were found to depend on the conditions of sample preparation and on the Sn concentration. Between 80 and 225 K, the intensity of the 388 nm band increased while that of the 539 nm band decreased. According to Jaek *et al.*, this anti-parallel behavior of these emission bands supported the assumption about their correspondence to two different states of the same type of centers with a temperature-dependent probability of transition between the states.

Lehmann [6] and Yamashita and Asano [59] have also reported the green emission band ($\sim$ 539 nm) due to the Sn^{2+} center in CaS. The peak position of this emission band does not vary with Sn concentration, in contrast to what has been observed for Sb^{3+} and Bi^{3+} in CaS. Furthermore, the addition of a halide

Table 10. Spectral positions in the excitation and emission spectra of Pb-activated sulfides

		Excitation spectrum (nm)	Emission spectrum (nm)
MgS	300 K†	280, 307, 358	379
CaS	300 K‡	349	366
	80 K§	259, 292, 345	355, 364
	63 K¶	345	357, 365
SrS	80 K‖	275, 302, 351	368, 374
	63 K¶	351	371, 376

† Asano and Yamashita [57].
‡ Lehmann [6].
§ Asano *et al.* [56].
¶ Ellervee [52].
‖ Yamashita *et al.* [55].

ion as coactivator was found to increase the intensity of the green emission band [6].

In the excitation spectrum the peak-positions of the Sn-induced bands reported by various workers agree with each other (Table 11). The excitation bands are referred to as *A*, *B* and *C* bands, respectively, by Yamashita and Asano, in accordance with the nomenclature for ns^2 ions [59]; but it has been speculated that the band at 299 nm is that due to a charge transfer transition [58].

Mössbauer and EPR spectra have helped to identify the presence of Sn centers in multiple charge states Sn^{2+}, Sn^{3+} and Sn^{4+} in the lattice. The EPR spectra, consisting of lines of paramagnetic absorption with $g = 2.0144$, showed a 300–700% increase in intensity after X-ray irradiation.

The addition of Na to Sn-doped CaS has been found to increase the intensity of the emission band at 636 nm. The results from Mössbauer and emission studies confirm the association of the bands at 539 and 636 nm with Sn^{2+} and Sn^{4+}–Na^+ centers, respectively [58].

4.9. *Antimony*

In CaS, Lehmann [6] has reported three absorption bands at about 318, 348 and 398 nm and a yellow–green emission band at 547 nm, attributed to substitutional Sb^{3+} ions in the lattice. The addition of monovalent alkali ions improves the emission efficiency slightly while the presence of a halide ion annihilates the Sb^{3+} emission in the lattice.

In a more detailed study, Yamashita [60] has also observed three excitation bands in CaS whose peak-positions are slightly different from Lehmann's results (Table 11). The emission spectrum consisted of the principal band at 545 nm with a shoulder at about 450 nm for low concentrations of the activator Sb^{3+} ion ($\leqslant 10^{-2}$ mol%). At high activator concentrations, the blue band disappeared. By resolving the emission spectrum into Gaussian curves, Yamashita has deduced a band at about 463 nm and had identified it as the reverse transition of the excitation band at 348 nm. The emission bands at 442 and 545 nm were also associated with the reverse transitions of the excitation bands at 318 and 398 nm, respectively. These identifications of the emission bands at 442 and 463 with the Sb^{3+} ion seem to be speculative and more work is required before anything conclusive can be said.

Table 11. Spectral positions in the excitation and emission spectra of Sb- and Sn-activated sulfides

	Excitation spectrum (nm)	Emission spectrum (nm)
Sb^{3+}		
CaS, 300 K†	318, 348, 398	547
80 K‡	322, 346, 393	545
Sn^{2+}		
CaS, 300 K†	301, 363	539
80 K§	253, 299, 359	539
80 K§	253	388
77 K¶	311, 332, 364	545
Sn^{4+}–Na:		
CaS, 80 K§	264, 302, 335, 370	636

† Lehmann [6].
‡ Yamashita [60].
§ Jaek *et al.* [58].
¶ Yamashita and Asano [59].

4.10. *Gallium and indium*

Gallium in CaS induces an emission band at about 869 nm which shifts to higher energy with the addition of either Cu or Ag in the lattice. On the other hand, the In-activated CaS emits a weak orange emission. Addition of either Na or K shifts the emission peak to about 550 nm and enhances the emission intensity. Addition of Cu or Ag does not introduce any new bands into the emission spectrum of In-activated sulfides [6].

4.11. *Zirconium*

Rawat and Ranade [61] have reported that Zr in CaS induces emission bands at about 450 and 640 nm, contrary to Lehmann's observation that CaS : Zr is non-luminescent. In SrS, Sivaraman and Sinha have also reported two bands with peaks at 470 and 560 nm [62]. Later, Bhatt *et al.* [63] observed an additional band at 639 nm and tried to interpret the results in terms of multiple valence states of Zr in the lattice.

4.12. *Scandium, yttrium and lanthanum*

All these three activators require the addition of a halide ion as coactivator and a reducing atmosphere for their incorporation into CaS. The emission spectra of Y- and La-activated CaS are similar to each other in shape with peaks at 444 and 487 nm respectively, while Sc induces a band at about 569 nm in CaS [6].

4.13. *Rare earths*

Sulfides activated with rare earths, particularly cerium and europium, have been the subject of detailed spectroscopic studies because of their potential as efficient phosphor materials for cathode-ray tubes, multicolor electroluminescent displays and fast high-resolution optically-stimulated luminescence imaging [3, 10, 64]. In this section we will discuss information on the physical aspects of rare-earth centers and their level positions in sulfides.

4.13.1. *Cerium.* Ce-activated CaS is a well-known fast-decaying green phosphor whose cathodoluminescence efficiency is comparable to that of the best green ZnS-phosphors [64]. Ce induces two emission bands at about 525 and 590 nm in MgS, 523 and 590 nm in CaS and 485 and 545 nm in SrS, respectively [7]. These emission bands have been assigned to transitions from the $5d$ state to $4f(^2F_{7/2}, ^2F_{5/2})$ states of the Ce^{3+} ion. Since the $4f$ state is shielded from the influence of the surroundings, the crystal field causes only a small perturbation of the $4f$ state, which is

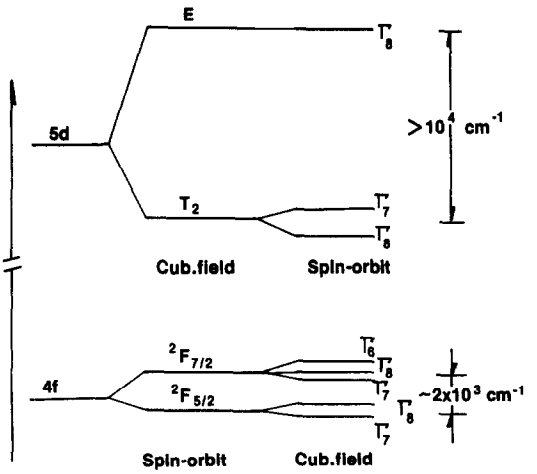

Fig. 10. Schematic energy level diagram of Ce^{3+} in a cubic crystal field (Hoshina [77]).

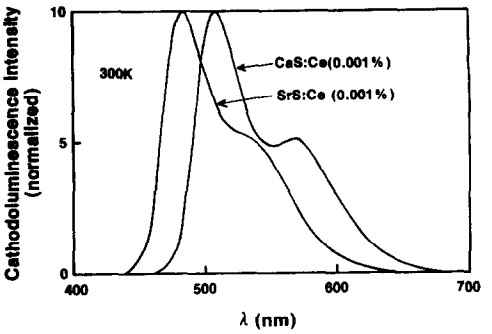

Fig. 11. Emission spectra of CaS : Ce (0.001 mol%) and SrS : Ce (0.001 mol%) (Okamoto and Kato [66]).

negligible in comparison with spin–orbit interaction (Fig. 10). The energy separation between the $^2F_{5/2}$ and $^2F_{7/2}$ levels of the $4f$ state in sulfides remains, therefore, approximately the same as in the free ion (Table 12). On the other hand, the $5d$ state is sensitive to the crystal field and strongly couples with the lattice vibrations. The optical transition, $5d \rightarrow 4f$ is therefore assisted by phonons and gives rise to broad emission bands as observed (Fig. 11). In the excitation spectrum the band at about 480 nm in MgS and 455 nm in CaS has been assigned to the $4f(^2F_{5/2}) \rightarrow 5d(^2T_{1g})$ transition while the band at about 254 nm in MgS is attributed to the transition $4F(^2F_{5/2}) \rightarrow 5d(^2E_g)$ [65].

In the emission spectra of Ce-activated sulfides, the peak positions of the emission bands vary little with the cerium concentration or with temperature [7]. For example, the band shifted to longer wavelengths from 504 to 516 nm as the cerium concentration increased from 10^{-4} to 10^{-2} mol% in CaS [66].

Both the excitation and emission spectra exhibit phonon structures superposed on a broad band at low temperatures ([65, 67], Fig. 12). Table 13 lists the observed zero-phonon lines in Ce-activated sulfides along with their suggested assignments. However, Blasse disagrees with this interpretation of the zero-phonon lines [68]. According to him, these lines are separated over a large energy range ($\sim 100\,cm^{-1}$) indicating the presence of various kinds of Ce centers in CaS.

In an EPR study, Wagner and Murphy have observed that the substitutional Ce^{3+} ions occupy sites of cubic and orthorhombic symmetry in roughly equal concentration [69]. This indicates that for half the Ce^{3+} ions the charge compensation is remote resulting in an isotropic g-value and that for the other half it is nearby yielding an anisotropic g-value. Table 14 lists the g-values obtained in CaS : Ce (0.05%) at 4.2 K. In the EPR spectrum the high symmetry directions of the principal axes along [001], [1$\bar{1}$0], and [110] and the orth orthorhombic symmetry

Table 12. Spectral positions in the excitation and emission spectra of Ce- and Eu-activated sulfides

			Excitation spectrum (nm)	Emission spectrum (nm)
Ce^{3+}:	MgS,†	300 K	254, 480	525, 590
	CaS,‡	300 K	454	523, 590
	SrS,§	300 K	—	485, 545
	SrS,¶	77 K	—	493, 533
Eu^{2+}:	MgS,‖	300 K	—	592
		80 K	251, 489	592
	CaS,‡‖	300 K	Broad (410–590)	652
		80 K	267, 495	654
	SrS,††	300 K	—	617
	SrS,¶	300 K	—	598
		77 K	—	611
Eu^{3+}:	SrS,‡‡	300 K	—	338

† Asano *et al.* [65].
‡ Lehmann and Ryan [7].
§ Okamoto and Kato [66].
¶ Keller and Pettit [73].
‖ Nakao [74].
†† Kato and Okamoto [75].
‡‡ Keller [76].

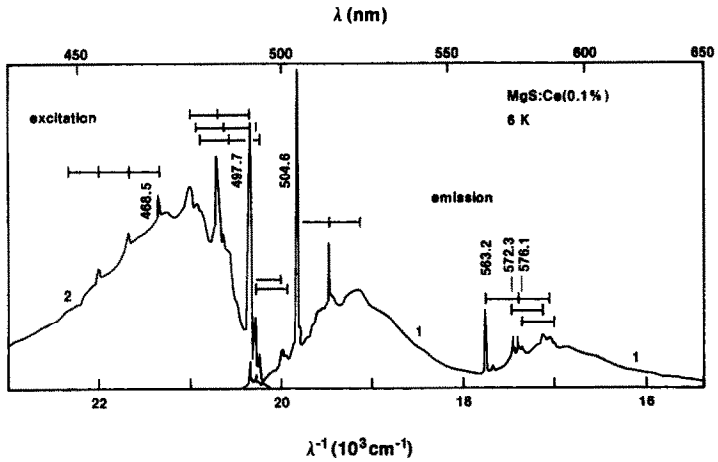

Fig. 12. Emission and excitation spectra of MgS : Ce (0.1 mol%) at 6 K (Asano *et al.* [65]).

suggest that the Ce centers are most probably due to the substitutional Ce^{3+} associated with charge compensation at the nearest-neighbor Ca^{2+} site in the [110] direction. The compensator could be a monovalent ion or a calcium vacancy. The fact that cubic and orthorhombic sites are equally populated tends to indicate that orthorhombic centers are due to calcium vacancies being nearby. In this way a single calcium vacancy compensates one Ce^{3+} locally and one Ce^{3+} distantly.

For concentration ranges from 10^{-4} to 0.5 mol% of Ce, CaS does not show the well-known concentration-quenching phenomenon, suggesting either that the energy exchange between Ce ions in the lattice has a lower probability than the radiative transition or that the solubility of Ce in CaS is low. However, Ce emission in CaS is characterized by a small Stokes shift ($\sim$0.4 eV) implying an overlapping of excitation and emission bands. This overlapping can facilitate efficiently the energy exchange between Ce ions in the lattice. It is therefore likely that the low solubility of Ce in CaS is responsible for its efficiency at high concentrations. Furthermore, X-ray diffraction patterns indicated the presence of a CeS phase in CaS when the Ce concentration was about 0.1 mol% [70]. The solid solubility limit of Ce as an emission center in CaS is therefore likely to be less than 0.1 mol%.

Table 13. Positions of the zero-phonon lines in the excitation and emission spectra of Ce-activated sulfides (Asano *et al.* [65])

Transition	MgS (nm)	CaS (nm)
$\Gamma_7(^2F_{5/2}) \rightarrow \Gamma_7(^2T_{2g})$	468.5	454.2
	491.7	
$\Gamma_7(^2F_{5/2}) \leftrightarrow \Gamma_8(^2T_{2g})$	493.3	474.2
	494.1	
$\Gamma_8(^2T_{2g}) \rightarrow \Gamma_8(^2F_{5/2})$	504.6	484.2
$\Gamma_8(^2T_{2g}) \rightarrow \Gamma_8(^2F_{7/2})$	563.2	539.2
$\Gamma_8(^2T_{2g}) \rightarrow \Gamma_7(^2F_{7/2})$	572.3	545.4
$\Gamma_8(^2T_{2g}) \rightarrow \Gamma_6(^2F_{7/2})$	576.1	548.2

Chlorine which is not a charge-compensator ion for Ce^{3+} greatly aids its incorporation in the lattice [7, 71]. For example, the peak intensity of the 520 nm bands is increased about sevenfold by the addition of chlorine in CaS : Ce (0.001 mol%) [71]. On the other hand, the incorporation of alkali metal ions as coactivators has also provided high luminescence efficiencies [66, 72]. This result tends to refute Lehmann's observation that the presence of a halide ion is essential to efficient and strong Ce^{3+} emission in sulfides. A small shift of the peak position from 517 to 508 nm was observed with the addition of Na in CaS : Ce phosphor [66].

4.13.2. *Europium.* In Eu-activated sulfides the emission spectrum consists of a single emission band originating from the intraionic transitions in the Eu^{2+} ion (Table 12). The peak positions are at about 592 nm in MgS, 652 nm in CaS and 617 nm in SrS at room temperature. The peak positions remain unchanged for Eu^{2+} concentrations <0.1 mol% but shift to lower energies with decreasing temperatures. In SrS the shift was found to be about 0.04 eV between 300 and 77 K [73].

The excitation spectrum of Eu-activated sulfides consists of two main bands referred to as *A* and *C* at about 251 and 489 nm in MgS and 267 and 495 nm in CaS, respectively. With increasing concentration of Eu^{2+} ions, an additional band referred to as *B* at

Table 14. Spin-Hamiltonian parameters for Ce^{3+} and Eu^{2+} ion in sulfides

			g	*A* (10^{-4} cm^{-1})	
Ce^{3+}:	CaS,§	4.2 K	1.2983	—	
Eu^{2+}:	CaS,§	4.2 K	1.9927	30.5†	
	CaS,¶	77 K	1.990	30.35†	13.43‡
	MgS,	77 K	1.985	30.71†	13.51‡
	SrS,	77 K	1.991	30.82†	13.79‡

† Corresponding to ^{151}Eu nuclei.
‡ Corresponding to ^{153}Eu nuclei.
§ Wagner and Murphy [69].
¶ Nakao [74].

about 285 nm appears in both MgS and CaS. The A band was assigned to the transition $4F^7 \rightarrow 5d(T_{2g})$ and the C band to $4f^7 \rightarrow 5d(E_g)$ transitions. Nakao has calculated the value for $10Dq$, that is, the energy splitting of the $5d$ state of Eu^{2+} ion by the crystal field in the point-charge model. The $10Dq$ values are 19,500 and 18,750 cm^{-1} in MgS and CaS, respectively. In comparison, the $10Dq$ value in NaCl is found to be 12,120 cm^{-1} [74].

The Eu^{2+} emission may be described as $4f^6(^7F)5d \rightarrow 4f^6(^7F)4f = 4f^7(^8S)$. Thus the $4f^6$ core should be in the same ^7F state in both the initial and the final states for the transition. The transition probability of $5d \rightarrow 4f$ is then reduced by a factor of 1/49, since the initial state $4f^6$ core has 49 alternatives of ^7F as the final state [77]. The decay time of Eu^{2+} is therefore expected to be longer than that of Ce^{3+}. Hoshina has calculated the $5d$–$4f$ radiative transition probabilities of Ce^{3+} and Eu^{2+} in CaS using pure $5d$ and $4f$ wave functions. It has been suggested that Ce^{3+} has the largest radiative transition probability among the rare-earth ions exhibiting $5d$–$4f$ emission. However the calculated decay times of Eu^{2+} and Ce^{3+} in CaS show only qualitative agreement with the experimental values of 36 and 750 ns, respectively [77].

The EPR spectrum of Eu^{2+} was found to be extremely complicated owing to the hyperfine interaction with the almost equally abundant ^{151}Eu and ^{153}Eu isotopes in the lattice [69, 74]. Each isotope has a nuclear spin $I = 5/2$ and hence two sets of six equally-spaced lines located around $g = 2$ are observed (Fig. 13). Table 14 lists the values of g and A

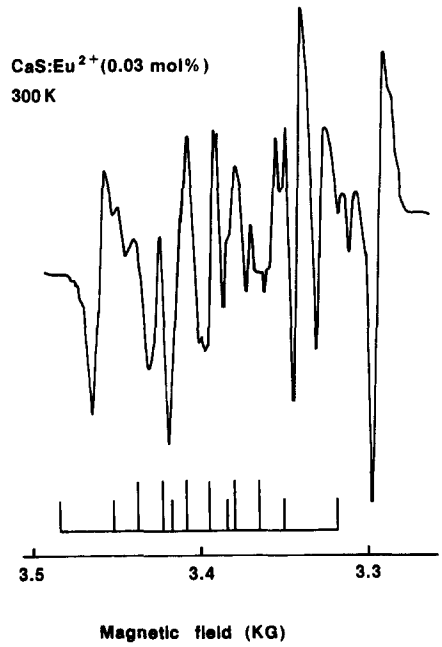

Fig. 13. EPR spectrum of CaS : Eu at 300 K. Schematic pattern at the bottom shows the observed positions of ^{151}Eu (short lines) and ^{158}Eu (long lines) (Nakao [74]).

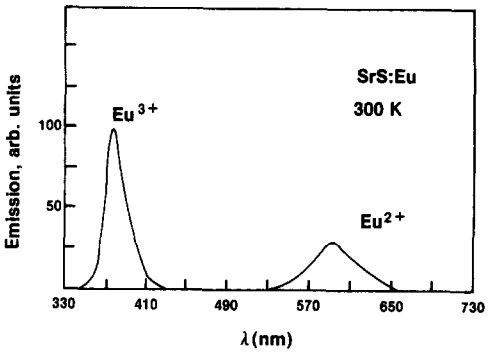

Fig. 14. Emission spectra of SrS : Eu containing both Eu^{2+} and Eu^{3+} (Keller [76]).

obtained in Eu-activated sulfides. In CaS the g-value does not show any variation with temperature on going from 77 to 4.2 K. It has been concluded that Eu^{2+} incorporates in the lattice substitutionally by replacing the host cation.

In SrS, Keller has studied the variation of the valence state of Eu using EPR and emission spectra [76]. Preparing the phosphor in a reducing atmosphere produced Eu^{2+} with an emission band at 592 nm, while preparation in an oxidizing atmosphere produced decreasing amounts of Eu^{2+} and increasing amounts of Eu^{3+} in the lattice (Fig. 14). A dominant peak located at 380 nm was associated with the Eu^{3+} in SrS. In CaS the emission intensity of Eu^{2+} was found to be enhanced by the presence of Ce^{3+} [7]. This may be due to the fact that the Ce^{3+} emission overlaps with the broad absorption band of Eu^{2+} in CaS and therefore the emission emanating from a Ce^{3+} ion will immediately be absorbed by a neighboring Eu^{2+} ion and reappear as Eu^{2+} emission in the lattice.

There have been very few reports on the other rare-earth activators in sulfides. Table 15 summarizes the spectral positions in the emission spectra taken mainly from the work of Lehmann on CaS [6] and Keller and Pettit on SrS [73]. However, the work so far reported on the absorption spectrum is limited to CaS only. At room temperature, the absorption spectrum consisted of a broad band showing structure in cases of Pr^{3+}-, Sm^{2+}-, Er^{3+}- and Yb^{2+}-activated CaS only [6]. Figure 15 shows both the absorption and emission spectra of Tb-activated CaS.

In CaS the rare earths, namely samarium and ytterbium were identified to exist in both the trivalent and divalent states. The EPR spectrum of Yb-activated CaS consisted of the signal at $g = 2.579$ due to the Yb^{3+} in the lattice. The hyperfine interaction A was found to be 69.9×10^{-4} and 19×10^{-4} cm^{-1} for ^{171}Yb and ^{173}Yb nuclei, respectively [78].

The emission spectrum of Sm^{3+}-activated sulfides consists of six group of lines at about 565, 605, 650, 710, 790, and 900 nm at 300 K [79]. The peak positions vary little with the host lattice and are found

Table 15. Spectral positions in the emission spectra of rare-earth activators in sufildes†

			Emission spectrum (nm)
Pr^{3+}:	CaS,	300 K	497, 671, 1184
	SrS,	300 K	501, 540
		77 K	421, 494, 498, 499, 502, 508, 512, 516
Nd^{3+}:	CaS,	300 K	—
	SrS,	300 K	485, 548
		77 K	478, 550
Sm^{3+}:	MgS,	300 K‡	565, 605, 650, 710, 790, 900
	CaS,	300 K	
	SrS,	300 K	
	BaS,	300 K	
Gd^{3+}:	CaS,	300 K	309, 315, 319, 557, 562, 586, 592
	SrS,	300 K	531
		77 K	429, 532
Tb^{3+}:	CaS,	300 K	381, 414, 438, 491, 550, 586, 622
	SrS,	77 K	382, 414, 439, 444, 457, 478
			496, 552, 589, 627
Dy^{3+}:	CaS,	300 K	486, 582
	SrS,	77 K	490, 495, 574, 578, 585, 589
Ho^{3+}:	CaS,	300 K	425, 493, 545, 592, 672
	SrS,	77 K	428, 462, 497, 548, 598
Er^{3+}:	CaS,	300 K	387, 412, 527, 557
	SrS,	77 K	390, 413, 493, 562
Tm^{3+}:	CaS,	300 K	474, 483, 661
		300 K	467, 471, 476, 480, 484, 487
			719, 733, 743, 758
	SrS,	77 K	491, 493, 495, 504
Yb^{3+}:	CaS,	300 K	Infrared
	SrS,	77 K	522
Yb^{2+}:	CaS,	300 K	748
Lu^{3+}:	SrS,	77 K	439, 491, 545

† Spectral levels are taken from Lehmann [6] for CaS and from Keller and Pettit [73] for SrS.
‡ Yamashita and Asano [79].

to shift slightly towards shorter wavelengths with the increase in the lattice spacing of the host material. By comparing the observed Sm^{3+} emission spectrum with that of Sm^{3+} in dilute acid solution, Yamashita and Asano have identified the first five groups as the transitions from the $^4G_{5/2}$ state to ^6H_J ($J = 5/2, 7/2, 9/2, 11/2, 13/2$) states and the last group as the $^4G_{5/2} \rightarrow {}^6F_J$ ($J = 1/2, 3/2, 5/2$) transitions. Furthermore, they have associated the line structure in the excitation spectrum to the transitions within the $4f^5$ configuration and the broad bands to the $4f^5 \rightarrow 4f^4 5d$ transition of Sm^{3+} in sulfides [79].

In SrS, Keller and Pettit have constructed energy level diagrams to gain information about the symmetry of rare-earth sites and have suggested that all

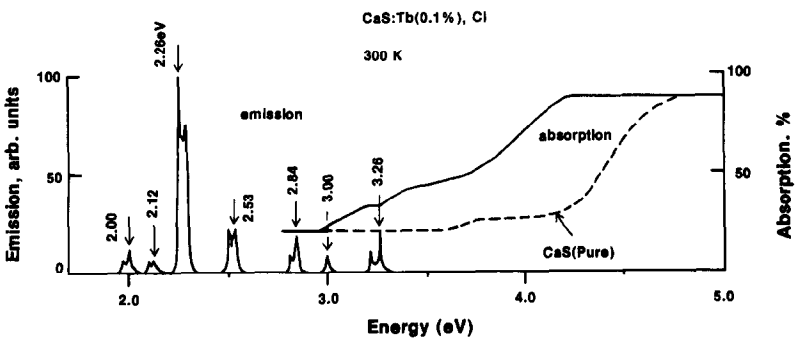

Fig. 15. Emission and absorption spectra of CaS : Tb (0.1 mol%), Cl at room temperature (Lehmann [6]).

the rare earths except Pr and Nd occupy substitutional sites.

Finally, rare-earth induced emission in CaS was found to obey three different decay laws, namely exponential, hyperbolic and power laws [6]. As is to be expected, the rare earths Pr^{3+}, Sm^{3+}, Gd^{3+}, Tb^{3+} and Tm^{3+} decay exponentially indicating a first-order process of electron recombination from one to another of the various $4f$-levels of the particular ions. For cases such as Ce^{3+}, Eu^{2+} and Yb^{2+}, where the electron transition responsible for the emission is not confined to the $4f$-shell of the ions, a hyperbolic law is followed indicating a second-order process. However, the ions Dy^{3+}, Ho^{3+} and Er^{3+} (which are expected to follow an exponential law) were found to obey a power law, suggesting neither first- nor second-order processes.

5. CONCLUDING COMMENTS

It has been a long-standing goal of defect spectroscopy to establish a connection between the observed spectrum and the microscopic structure of a color center in materials. However, it is somewhat ironic that the intrinsic defect structure of sulfides has received rather little attention although there has been intense activity in impurity-activated sulfides. There remain many uncertainties about the basic aspects of defect centers resulting in an incomplete description of the various properties of sulfides.

For the purpose of constructing models of defects in alkaline-earth sulfides, there has been a tendency to look for possible analogies between sulfides and either alkali halides or zinc sulfides. Although sulfides share some of their physical properties with zinc sulfide, their ionicity is large enough that the rock salt behavior predominates. Hence, the results tend to support models that have been constructed for alkali halides. In the lattice, substitutional sites are preferred by impurities. However, the understanding of the principle of charge compensation in the lattice remains inconclusive. The (Schottky defect) vacancies are the easiest defects to form and therefore, in the absence of other chemical impurities, monovalent/trivalent impurities will be accompanied by the introduction of vacancies in the lattice. Furthermore, the procedure adopted in preparing the sulfides appears to have a profound influence on the microscopic structure of the various centers formed. This is reflected in the conflicting results reported both in emission and absorption for the same material by different workers. Finally, it is hoped that this brief account of the present status of spectroscopic properties of defects in sulfides will provide a stimulus for both experimental and theoretical investigations that will result in a complete microscopic description of the physics of these systems.

Acknowledgements—We acknowledge financial support for the preparation of this paper from the U.S. Department of Energy under grant No. DE-FG02-85-ERA45224. One of us (R.P.) has benefited from many discussions with P. K. Ghosh, and V. Shanker.

REFERENCES

1. Pandey R., Kunz A. B. and Vail J. M., *J. Mater. Res.* **3,** 1362 (1988); Yoshiyama H., Tanaka S., Mikami Y., Ohshio S., Nishiura J., Kawakami H. and Kobayashi M., *J. Cryst. Growth* **86,** 56 (1988).
2. Kaneko Y. and Koda T., *J. Cryst. Growth* **86,** 72 (1988).
3. Tanaka S., Shanker V., Shiki M., Deguchi A. and Kobayashi H., *SID International Symposium*, Orlando, Florida, p. 218 (1985).
4. Wosnitza J., Lohneysen H. V. and Zinn W., *Solid St. Commun.* **65,** 509 (1988).
5. Lenard P., Schmidt F. and Tomascheck R., *Handb. Exp. Phys.*, Vol. 23. Akademie Verlagsges, Leipzig (1928).
6. Lehmann W., *J. Luminesc.* **5,** 87 (1972).
7. Lehmann W. and Ryan F. M., *J. electrochem. Soc.* **118,** 477 (1971).
8. Holloway H. and Jesion G., *Phys. Rev.* **B26,** 5617 (1982).
9. RaO R. P. and RaO D. R., *Hlth Phys.* **45,** 1001 (1983).
10. Gaslot J., Braunlich P. and Fillard J. P., *Appl. Phys. Lett.* **40,** 376 (1982).
11. RaO R. P., *J. Mater. Sci.* **21,** 3357 (1986).
12. Philips, J. C., *Rev. mod. Phys.* **42,** 317 (1970).
13. Kaneko Y., Morimoto K. and Koda T., *J. phys. Soc. Japan* **51,** 2247 (1982).
14. Pandey R. and Harding J. H., *Phil. Mag.* **B49,** 135 (1984).
15. Kaneko Y. and Koda T., *J. Cryst. Growth* **86,** 72 (1988).
16. Realo K. and Jaek I., *Eesti NSV Teaduste Akad. Toimetised, Fuus Mat.* **27,** 79 (1978).
17. Thakur K. P. and Pandey J. D., *J. inorg. nucl. Chem.* **37,** 645 (1975).
18. Zollweg R. J., *Phys. Rev.* **111,** 113 (1958).
19. Auzins A., Ortan J. W. and Wert J. E., *Paramagnetic Resonance*, Vol. 1, p. 90. Academic Press, New York (1963).
20. Ghosh P. K. and Shanker V., *J. Luminesc.* **20,** 139 (1979).
21. Shanker V., Ghosh P. K. and Reddy T. R. S., *Ind. J. pure appl. Phys.* **14,** 193 (1976).
22. Ghosh P. K. and Pandey R., *J. Phys. C* **15,** 5875 (1982).
23. Kolopus J. and Lapeyre G., *Phys. Rev.* **176,** 1025 (1968).
24. Ekbote S. N. and Ranade J. D., *Ind. J. Phys.* **46,** 529 (1972).
25. Rebane K. S., Ots A. and Voolaid H., *J. Luminesc.* **11,** 271 (1975).
26. Henderson B., *CRC Crit. Rev. solid St. Mater. Sci.* **9,** 1 (1980).
27. Efanova E. P. and Mikhailin V. V., *Moscow Univ. Phys. Bull. (U.S.A.)* **36,** 31 (1981).
28. Allsalu M. L., Mikhailin V. V., Pedak E. Yu., Rozhdestvenskii M. A. and Tereschenko I. V., *Moscow Univ. Phys. Bull. (U.S.A.)* **38,** 84 (1983).
29. Kapoor Y. M. and Hensley E. B., *Phys. Rev.* **B23,** 5581 (1981).
30. Ghosh P. K. and Shanker V., *Ind. J. Phys.* **53A,** 203 (1978).
31. Ray B., Brightwell J. W., Allsop D. and Green A. G. J., *J. Cryst. Growth* **86,** 644 (1988).
32. Brightwell J. W., Ray B., Sephton P. and Viny I. V. F., *J. Cryst. Growth* **86,** 634 (1988).
33. Brightwell J. W., Ray B. and Buckley C. N., *J. Cryst. Growth* **59,** 210 (1982).
34. Allsalu M. L. Yu, Koz'menko M.V., Mikhailin V. V., Neuostrueva I. A. and Pedak E. Yu, *J. appl. Spectrosc.* **23,** 1120 (1975).

35. Sivaraman S. and Bhawalkar D. R., *Ind. J. pure appl. Phys.* **9,** 322 (1971).
36. Asano S., Yamashita N., Nakao Y. and Matsushima Y., *Phys. Status Solidi* (*b*) **108,** 229 (1981).
37. Ghosh P. K., Shanker V. and Reddy T. R. S., *Indian J. Phys.* **50,** 438 (1976).
38. Nair P. G., Lingam K. V. and Machwe V. G., *Proc. Indian Acad. Sci.* **Lxx,** Section A (1969).
39. Wagner G. R., Murphy J. and Rubenstein M., *J. Phys. Chem. Solids* **33,** 273 (1972).
40. Asano S., Yamashita N., Oishi M. and Omorik, *J. phys. Soc. Japan* **25,** 784 (1968).
41. Lehmann W., *J. electrochem. Soc.* **117,** 1389 (1970).
42. Laud B. B. and Kulkarni V. W., *J. Phys. Chem. Solids* **39,** 555 (1978).
43. Laud B. B. and Kulkarni V. W., *Phys. Status Solidi* (*a*) **51,** 269 (1979).
44. Ghosh P. K. and Jain K. L., *Indian J. pure appl. Phys.* **12,** 188 (1974).
45. Yamashita N. and Asano S., *J. phys. Soc. Japan* **40,** 144 (1976).
46. Asano S. and Yamashita N., *Phys. Status Solidi* (*b*) **97,** 311 (1980).
47a. Asano S. and Yamashita N., *Phys. Status Solidi* (*b*) **105,** 305 (1981).
47b. *ibid.* **105,** 613 (1981).
48. Asano S., Nakao Y., Yamashita N. and Matsuyama I., *Phys. Status Solidi* (*b*) **133,** 333 (1986).
49. Asano S. and Yamashita N., *Phys. Lett.* **86A,** 191 (1981).
50. Yamashita N., Iwasaki A., Asano A., Ohishi M. and Ohmori K., *J. phys. Soc. Japan* **53,** 4425 (1984).
51. Efanova E. P., *Moscow Univ. Phys. Bull.* (*U.S.A.*) **36,** 77 (1981).
52. Ellervee A. F., *Phys. Status Solidi* (*b*) **82,** 91 (1977).
53. Yamashita N. and Asano S., *Phys. Lett.* **96A,** 375 (1983).
54. Saxena R. C. and Ranade J. D., *Indian J. pure appl. Phys.* **7,** 817 (1969).
55. Yamashita N., Ohira T., Mizuochi H. and Asano S., *J. phys. Soc. Japan* **53,** 419 (1984).
56. Asano S., Yamashito N. and Nakao Y., *Phys. Status Solidi* (*b*) **89,** 663 (1978).
57. Asano S. and Yamashita N., *Phys. Status Solidi* (*b*) **108,** 549 (1981).
58. Jaek I., Realo E., Seman V. and Murk L., *Phys. Status Solidi* (*b*) **61,** 745 (1974).
59. Yamashita N. and Asano S., *J. phys. Soc. Japan* **41,** 536 (1976).
60. Yamashita N., *J. phys. Soc. Japan* **35,** 1089 (1973).
61. Rawat B. L. and Ranade J. D., *J. Luminesc.* **14,** 417 (1976).
62. Sivaraman S. and Sinha O. P., *Indian J. pure appl. Phys.* **10,** 131 (1972).
63. Bhatt N., Kamara P. C., Diwan P. S. and Sivaraman S., *Indian J. pure appl. Phys.* **14,** 1015 (1976).
64. Lehmann W. and Ryan F. M., *J. electrochem. Soc.* **119,** 275 (1972).
65. Asano S., Yamashita N. and Ohnishi T., *Phys. Status Solidi* (*b*) **99,** 661 (1980).
66. Okamoto F. and Kato K., *J. electrochem. Soc.* **130,** 432 (1983).
67. Asano S., Yamashita N. and Ogawa Y., *Phys. Status Solidi* (*b*) **118,** 89 (1983).
68. Blasse G., *Phys. Status Solidi* (*b*) **104,** k57 (1981).
69. Wagner G. R. and Murphy J., Report AD-760803, Westinghouse Research Laboratories (1973).
70. Kim G. C., Park H. L., Yun S. I. and Moon B. G., *J. Mater. Sci. Lett.* **5,** 359 (1986).
71. Pandey R. and Ghosh P. K., unpublished.
72. Vij D. R., Mathur V. K., Shanker V. and Ghosh P. K., *J. Phys. D* **29,** 1509 (1976).
73. Keller S. P. and Pettit G. D., *J. chem. Phys.* **30,** 434 (1959).
74. Nakao Y., *J. phys. Soc. Japan* **48,** 534 (1980).
75. Kato K. and Okamoto F., *Jap. J. appl. Phys.* **22,** 76 (1983).
76. Keller S. P., *J. chem. Phys.* **30,** 556 (1959).
77. Hoshina T., *J. phys. Soc. Japan* **48,** 1261 (1980).
78. Watts R. K., *Solid St. Commun.* **4,** 549 (1966).
79. Yamashita N. and Asano S., *J. phys. Soc. Japan* **56,** 352 (1987).
80. Pandey R., Jaffe J. and Kunz A. B., unpublished (1990).